Vol 17 No 7, July 2008
1674-1056/2008/17(07)/2683-06

Chinese Physics B

© 2008 Chin. Phys. Soc.
and IOP Publishing Ltd

Effect of fabrication conditions on the properties of indium tin oxide powders

Xie Wei(谢 卫)†

Engineering Institute of Engineer Corps, PLA Univ. of Sci. & Tech., Nanjing 210007, *China*

First Scientific Research Institute of Wuxi, Wuxi 214035, *China*

(Received 29 January 2008; revised manuscript received 27 February 2008)

This paper reports that indium tin oxide (ITO) crystalline powders are prepared by coprecipitation method. Fabrication conditions mainly as sintering temperature and Sn doping content are correlated with the phase, microstructure, infrared emissivity ε and powder resistivity of indium tin oxides by means of x-ray diffraction, Fourier transform infrared, and transmission electron microscope. The optimum sintering temperature of 1350°C and Sn doping content 6∼8wt% are determined. The application of ITO in the military camouflage field is proposed.

Keywords: tin-doped indium, sintering temperature, infrared emissivity, powder resistivity
PACC: 7280, 6110M, 8140

1. Introduction

Indium tin oxide (ITO) is a tin-doped indium oxide semiconductor material and is widely used as an infrared reflector and as a transparent electrode material.[1−5] The high infrared reflectivity of ITO leads to its use as a heat shielding material. Especially in the military camouflage field, materials with low infrared emissivity ε (i.e. high infrared reflectivity) are necessary.[6−8] Typically, materials which have a shiny or lustrous finish, such as metals, have a low thermal emissivity, a typical metallic lacquer having a thermal emissivity of about 0.5. Paints with metallic constituents are widely used in the automotive industry; however metallic material cannot provide good visual camouflage. Some common materials with matt finish have good visual camouflage, but have a high infrared emissivity.

In spite of the wide use of ITO semiconductors in many fields, the preparation and characterization of ITO is still an area of active research and development. Small changes in the preparation conditions and the annealing protocol can have profound effects on the properties of ITO samples. As a consequence, the preparation conditions for correlating the various properties in ITO are of great interest, both from a practical point of view and for basic research into this metal oxide material.

In this paper, the green ITO crystalline powders are synthesized by the coprecipitation method. The phase and microstructure of ITO at different sintering temperatures are characterized by means Fourier transform infrared (FTIR) spectroscopy, x-ray powder diffraction, and transmission electron microscope (TEM). Effects of sintering temperature and Sn doping content on the infrared emitting and electrical properties of ITO samples are analysed. And the optimum sintering temperature and Sn doping content are proposed.

2. Experimental

2.1. Preparation of ITO powders

Tin-doped indium oxide semiconductors were prepared by the coprecipitation with ammonium hydroxide of indium and tin hydroxides from appropriate mixtures of indium and tin chloride solutions in hydrochloric acid, followed by a washing procedure and heat treatment.

The $SnCl_4{\cdot}5H_2O$ and $InCl_3$ were separately dissolved in hydrochloric acid. The acid solutions were then mixed in desired proportions and diluted with distilled water to 8 times the original volume. The solution was maintained at 60°C on a steam bath and 3.5% ammonia solution was added dropwise until a PH of 8.5 had been achieved. The resulting mixed hydrox-

†E-mail: fcwzsq@163.com

ide precipitate was washed alternately with water until the washings showed no trace of chloride ion. The precipitate was then filtered, dried at 80°C, and ball-milled for 2h. Finally the powders were sintered under different temperatures and green ITO crystalline particles with different properties are formed.

2.2. Measurement

2.2.1. Infrared spectroscopy

The infrared spectroscopy of ITO samples prepared under different sintering temperatures was carried out using Nicolet AVATAR 360 FTIR.

2.2.2. X-ray diffraction (XRD)

The obtained crystalline phases and composition of the samples are identified by XRD (using Rigaku K/max 2550 VB/PC) made on an instrument equipped with a graphite monochlometer using CuKα radiation.

2.2.3. The morphology analysis

The morphology of ITO crystalline particles was observed on high resolution transmission electron microscope (TEM) (JEM-1200EX II type made by Japan).

2.2.4. Volume resistivity

The volume resistivity of ITO samples was measured by the Intelligent Electric Bridge. The ITO samples under test were first pulverized and compressed into cylindrical shape with 1cm diameter and 1cm height. The resistivity of ITO powder was deduced from its volumetric resistance according to the formula

$$\rho = R\frac{A}{L}.$$

Here, $\rho \sim$ the resistivity of samples.

$R \sim$ the volume resistance.

$A \sim$ area of the cylinder.

$L \sim$ height of the cylinder.

2.2.5. Infrared emissivity analysis

In order to measure the infrared emissivity of ITO samples, the film-forming binder with high infrared transparency is specially synthesized.[9] ITO sample and binder with the weight ratio of 1 to 1 are blended together in the mill boxer, thoroughly grounded and dispersed. The pressure-fed spray gun is used to spray the paint onto a copperplate paper. The thickness of the coating is thick enough to exclude the influence of the copperplate paper on the infrared emissivity ε. After the coating is sufficiently dried, its thermal infrared emissivity ε in the 8–14μm is measured. IRE-1 Infrared Emission Thermometer is used to measure the thermal infrared emissivity ε of coatings under the temperature 50°C.

3. Results and discussion

3.1. FTIR analysis

The infrared spectroscopy of the coprecipitate of In with Sn prepared at the temperatures 120°C, 160°C, 240°C and 350°C is shown in Fig.1. For all samples sintered at temperatures lower than 300°C, two absorption peaks appear around 3300cm^{-1} and 1630cm^{-1}, which correspond to the stretching and bending vibrations of OH bond respectively. The stretching vibration peak of OH bond is broader, and may result from the hydrogen bond existing in the molecules. When the sintering temperature is increased to 240°C, the stretching vibration peak of OH bond is shifted to 3500–3550cm^{-1}, and the absorption peak sharpens, which means that the associated hydroxy disappears. With increasing of sintering temperature to above 300°C, the stretching and bending vibration peaks all disappear, which means that the coprecipitate of In with Sn hydroxide turns to ITO.

Also it is shown that two absorption peaks corresponding to the bridged OH and the tail OH in the vicinity of 1100cm^{-1}[10] are observed for the samples sintered at 120°C and 160°C. With increasing sintering temperature, the hydroxide of indium with tin turns to ITO, and correspondingly the intensity of the two absorption peaks declines. When the sintering temperature is increased to 240°C, the absorption peak around 1160cm^{-1} first disappears because the bridged OH is easier to break off or even to form the tail OH. When the sintering temperature is further increased to 350°C, the absorption peak around 1076cm^{-1} also disappears.

Also, the absorption peak around 502cm^{-1} for the samples sintered at 120°C and 160°C corresponds to In–O bond.[11,12] When the sintering temperature is increased above 230°C, the absorption peak disappears, while a strong absorption peak corresponding

to In–O–In bond around 417cm^{-1} appears.

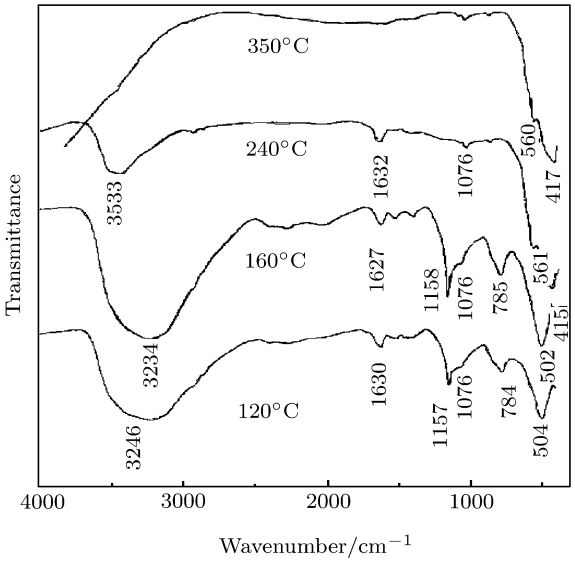


Fig.1. Infrared absorption spectra of samples.

3.2. XRD analysis

In order to qualify the phase and microstructure of the coprecipitate of In with Sn hydroxide sintered at different temperatures, XRD analysis is performed. Figure 2 shows XRD patterns of ITO samples sintered at 1350°C with Sn content of 6wt%, 8wt%, and 10 wt% respectively. XRD of Pure SnO_2 is also shown in Fig.2

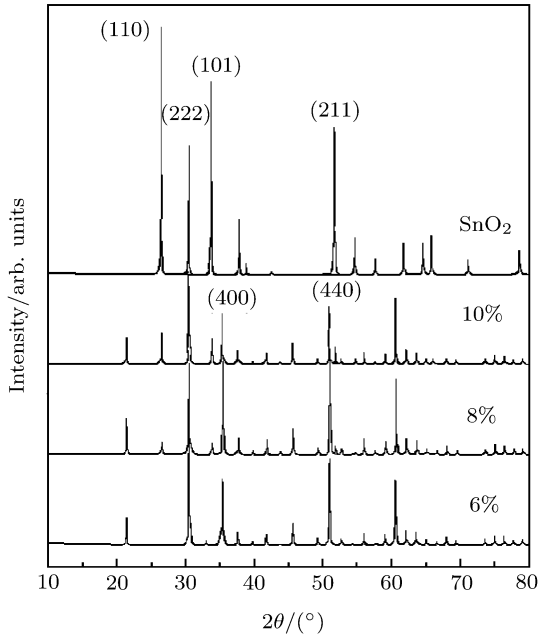


Fig.2. XRD of ITO sintered at 1200°C with different Sn content.

for contrast. XRD pattern of ITO specimen with Sn content of 6wt% is similar to that of In_2O_3 with the body centred ferro-manganese structure. No diffraction peak of pure SnO_2 occurs due to the substitutional incorporation of Sn^{4+} ions at In^{3+} sites. When Sn content is 8wt% or more, the diffraction peaks of SnO_2 appear. Three strong diffraction peaks correspond to the crystalline faces (110), (101), and (211) of the cubic structured SnO_2. With the Sn content increasing further, the diffraction peak intensity rises gradually. It makes clear that the Sn doping limit is between 6wt% and 8wt%. With increasing Sn content above 8 wt%, Sn will dissociate from the crystalline lattice of ITO.

Figure 3 shows XRD patterns for these samples with the same 7wt% Sn doping content sintered at 160°C, 350°C, 700°C, 1200°C and 1350°C respectively. XRD patterns of the ITO samples sintered at 160°C resemble the cubic structured $In(OH)_3$. When the sintering temperature is increased above 350°C, the sample gives a XRD pattern similar to the body centred ferro-manganese structured In_2O_3, which means that indium-tin hydroxide have led to ITO completely. The peaks are little shifted because of Sn doping.

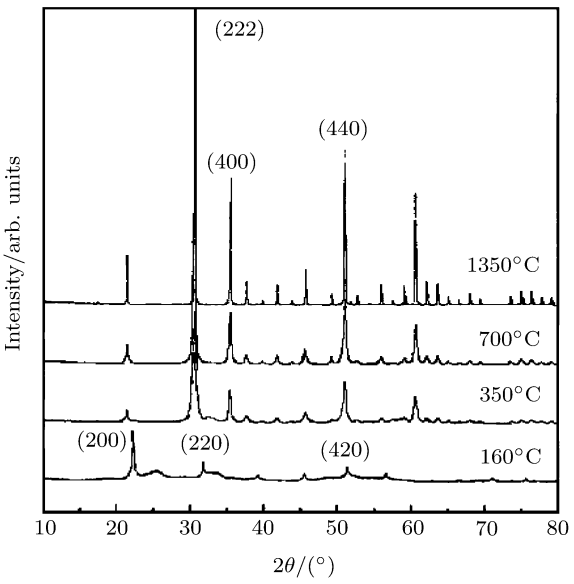


Fig.3. XRD patterns of samples sintered at different temperatures.

The very presence of XRD lines indicated that the semiconductors are microcrystalline in nature rather than glassed. With increasing the sintering temperature, the mean dimension of the microcrystals, D, is

calculated using Scherer's formula:

$$D = \frac{kl}{h_{1/2}} \cos\theta.$$

Where $h_{1/2}$ is the corrected width of the diffraction peak at half height, λ is the wavelength of the x-ray, and θ is the diffraction angle. Since the uncertainty in determining the diffraction broadening increases with increasing crystal size, D values for the high temperature samples are not very accurate. Results of the measurements are given in Table 1.

Table 1. The grain size D and the ratio of diffraction peak intensities.

specimens	T/°C	Ratios of diffraction peak intensities			D/nm
		(400)>/(222)	(440)/(222)	(622)/(222)	
ITO1	350	0.28	0.35	0.23	8
ITO2	700	0.29	0.32	0.21	13
ITO3	1000	0.30	0.35	0.26	15
ITO4	1200	0.32	0.38	0.29	30
ITO5	1350	0.32	0.39	0.29	65

It is shown from Table 1 that with increasing sintering temperature, the mean size of the microcrystalline increases. When the sintering temperature is below 1000°C, the mean size of the microcrystalline increases slowly. When the sintering temperature increases further, the crystallization of ITO is more complete, and the mean size of the microcrystalline grows fast. For ITO samples sintered at 1200°C, the crystalline structure is more perfect, and the grain symmetry is changed no more.

3.3. TEM analysis

Figure 4 gives the TEM of ITO samples sintered at 1350°C. Every grain is an independent ellipsoid and the average particle size is 300nm. The result is larger than that of the results calculated by XRD. It is probably because that x-ray gives the mean size of the microcrystalline and TEM gives the average size of the particle consisting of a lot of microcrystallines.



Fig.4. The micrograph of ITO crystalline particles.

3.4. The powder resistivity

Figure 5 shows the effect of the sintering temperature on the powder resistivity. With increasing the sintering temperature, the powder resistivity decreases rapidly, and attains a minimum at the sintering temperature of 1300–1400°C. The powder resistance includes three parts, the inherent resistance of particles, the contact ohmic resistance between particles constituting the powder, and the potential barrier resistance across grain boundaries. When the sintering temperature is lower, the doping reaction is not complete and the crystalline structure is not perfect, which results in lower carrier concentration. Therefore the inherent resistance of particles is relatively high. With the increasing sintering temperature, the effect of doping is improved and more Sn^{4+} replaces In^{3+} constituting the In_2O_3 lattice. The concentration of conducting carriers is increased, therefore the inherent resistance is lowered quickly. Also with increasing sintered temperature, the grain size grows, the crystal structure is more perfect, and the porosity of the sample is lowered. Therefore the contact resistance and the potential barrier resistance are lowered, and the resistivity is correspondingly lowered.

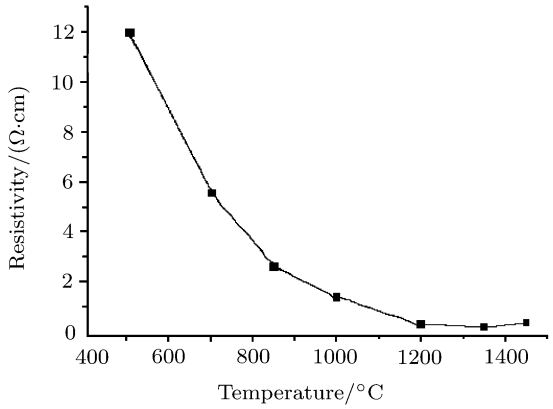


Fig.5. Effect of the sintering temperature on the powder resistivity.

Figure 6 shows the effect of Sn doping content on the powder resistivity. When the dopant concentration is less than 7wt%, the volume resistivity decreases with increasing Sn doping concentration. As analysed above, the introduction of Sn^{4+} will increase the carrier concentration. Therefore the volume resistivity is lowered. When the dopant content is higher than 7wt%, the volume resistivity increases with increasing Sn doping content. The crystalline In_2O_3 has body centred ferro-manganese structure, the average coordination number of In^{3+} is $\frac{16}{3}$.[12] If a substitutional Sn^{4+} ion lies in the lattice sites of $\frac{16}{3}$ In^{3+} ions which are in the vicinity of a substitutional Sn^{4+} ions, non-conducting SnO_2 is probably formed and dissociates from the crystal lattice. Therefore the volume resistivity increases with the dopant content which is higher than 7wt%.

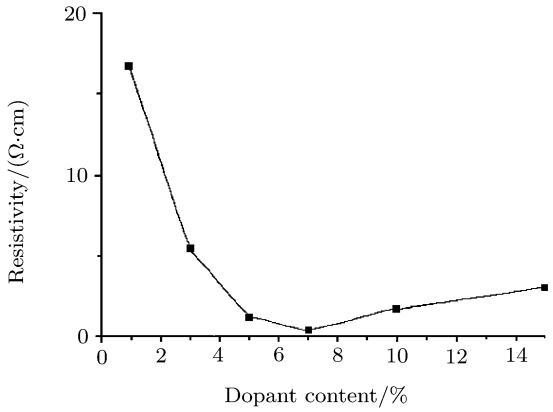


Fig.6. Effect of Sn doping content on the powders resistivity.

3.5. Infrared emissivity analysis

Figure 7 gives the influence of the sintering temperature on the infrared emissivity ε of ITO coatings. With increasing the sintering temperature continuously to 1000°C, ε begins to decrease. When the sintering temperature increases to 1350°C, ε is reduced to its minimum value 0.68. With increasing the sintering temperature further, ε begins to rise. Therefore the optimum sintering temperature is between 1300–1350°C for fabricating ITO crystalline particles with low infrared emissivity.

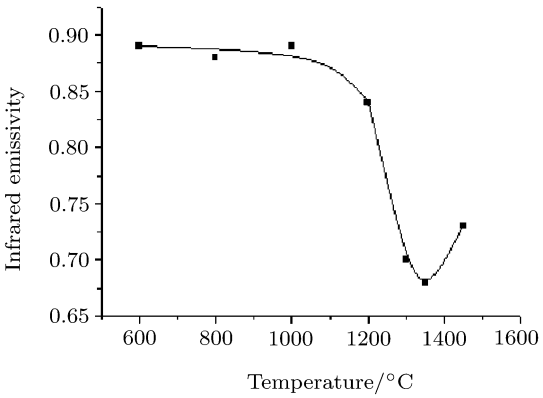


Fig.7. Effect of the sintering temperature on the infrared emissivity.

Figure 8 shows the influence of Sn doping content on the infrared emissivity ε. With increasing Sn doping content, Sn^{4+} will substitute In^{3+} in the crystalline structure of In_2O_3, more free carriers are formed and the infrared emissivity is reduced. When Sn doping content increases to 8wt%, the infrared emissivity ε is reduced to its minimum value 0.74. If further increasing Sn doping content to higher than 8wt%, a new crystalline structure $In_4Sn_2O_3$ will be formed and leads to the decreasing of the carrier concentration, so the infrared emissivity ε will even increase.

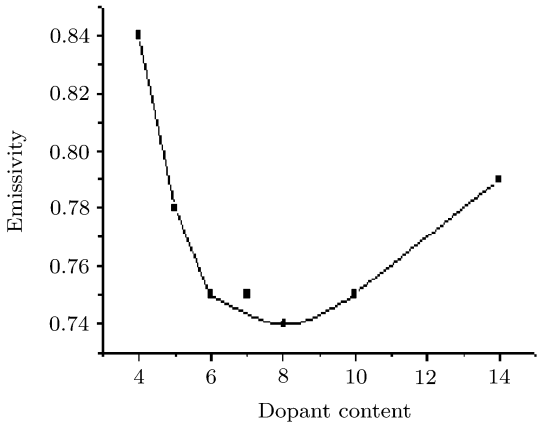


Fig.8. Effect of Sn doping content on the infrared emissivity.

4. Conclusions

Sintering temperature and Sn doping content determine the properties of ITO. With increasing the sintering temperature, the size of the microcrystalline grain of ITO increases. And when the sintering temperature increases to 1350°C, the crystallization process is complete and the crystalline structure is perfect. The same effect of sintering temperature on the infrared emissivity and powder resistivity of ITO is observed, and the optimum sintering temperature for fabricating lower powder resistivity and lower infrared emissivity ε is 1350°C.

XRD, powder resistivity and infrared emissivity measurements show that the optimum Sn doping limit is 6–8wt%. With increasing doping content, nonconducting SnO_2 is formed, which results in the increase of powder resistivity.

References

[1] Purvis K. G., Schwartz J and Bernasek S 2000 *J. Am. Chem. Soc.* **122** 1808

[2] Zhang W J and Wang T M 2004 *Acta Phys. Sin.* **53** 1924 (in Chinese)

[3] Oh S and Han S 2000 *Langmuir* **16** 6777

[4] Scott H B and Stefan F 2002 *J. Alloys and Compounds* **338** 73

[5] Cheng S H, Ning Z Y and Huang F 2002 *Acta Phys. Sin.* **51** 668 (in Chinese)

[6] Brunswick C 1995 *Guide to Camouflage for DARCOM Equipment Developers, Report Prepared for MERADCOM under Contract DAAG* 53-76-C-0126

[7] Raisbeck G, Aronson J R and Key M E 1997 *Design Goals for Future Camouflage Systems* AD-A099-223

[8] Lofgren Per-Ake 1987 *Camouflage Concepts for the Nineties, Proceedings of the International Conference on Polymers in Defence* **17** 1

[9] Fu C W and Chen M Q 2008 *Chin. Phys.* B **17** 1107

[10] Li Q S, Zhang J Z and Song L 2002 *J. Inorg. Mater.* **17** 489

[11] Nakamoto K 1970 *Infrared and Roman Spectra of Inorganic and Coordination Compounds* 3rd edn (New York: Wiley)

[12] Fan Z X, Sun Y C and Chen J L 2002 *Chin. J. Semiconductors* **22** 1382 (in Chinese)